Finite Element Modeling of Plain Weave Composites for Flexural Failure

Ömer Soykasap

Afyon Kocatepe University, Faculty of Technical Education,

A.N.S. Campus, 03200 Afyonkarahisar, Turkey

soykasap@aku.edu.tr

Keywords: plain weave composite, finite element modeling, flexure failure

Abstract. In this paper, flexural failure of plain weave composites is studied using finite element modeling. Initially curved beam elements are used to model the warp and weft yarns of the unit cell of the plain weave composite. The effective material properties are obtained by the finite element model with periodic boundary conditions. The flexural failure of a single-ply plain-weave T300/LTM45 composite is estimated based on homogenized material properties.

Introduction

Macro-mechanical properties of a woven composite depend on properties of fibre and matrix and their interactions. Material behavior of woven composites is quite different from that of unidirectional laminates, in which classical lamination theory (CLT) has been used. There are several homogenizing schemes available in the literature based on analytical and numerical techniques [1-6]. In CLT macro-mechanical properties of a laminate is obtained integrating the in-plane properties of a single ply through the thickness. Direct application of CLT to woven composites yields significant errors. Although in-plane properties of these materials can be estimated accurately using CLT and its adapted forms, the corresponding bending properties lack accuracy particularly for one- or two-ply woven laminates. Recently Soykasap [7] obtained material properties of plain weave composites using finite element (FE) modeling. Initially curved beams were used to model resin infiltrated fiber bundles. It was estimated that direct application of CLT or adapted form of CLT using a mosaic model could result in errors of up to 200% in the maximum bending strains or stresses, and up to 400% in the bending stiffnesses. Karkkainen and Sankar [8] carried a FE analysis of a plain weave composite using representative volume element for failure initiation. Direct micromechanics method yielded higher flexural stiffnesses as much as a factor of 2.9 compared to the results of FE analysis.

This paper presents FE analysis for flexural behavior of woven composites considering the fiber and the matrix and their interactions. FE model using Abaqus program [9] is developed to predict the bending properties of plain-weave T300/LTM45 composite. Initially curved beam elements are used to model each infiltrated fiber bundle. The interlaced yarns are constrained at the crossover points kinematically, representing the bonding between the yarns, and transferring loads from one yarn to another. Kinematic constraints are imposed at the coupling nodes of the crossover points. Previous finite model studied by Soykasap [7] is extended to include periodic boundary conditions after successful application of a similar model for triaxially woven composites by Kueh and Pellegrino [10]. Geometrically nonlinear analysis of the model with periodic boundary conditions is carried out in order to obtain homogenized stiffnesses of the composite. The results of FE model are compared with published data.

Material Properties

In a plain weave composite longitudinal and transverse yarns (called warp and weft) pass over and under each other alternately (see Fig.1). The macro structure of the composite can be obtained by

assuming a repeating cell which is the smallest unit of the composite, and adding the unit cells longitudinally and transversely as many as needed. The unit cell consists of only two warp and weft yarns. The macro-mechanical properties of the composite can be estimated considering the unit cell. The composite is assumed to be balanced when the number of resin infiltrated fibres in warp and weft direction is equal, and hence material properties in both directions are the same. Plain-weave carbon reinforced plastic T300/LTM45 is considered for modeling [7]. T300/LTM45 has a fibre volume fraction of V_f=0.5, an areal density of 94 g/m^2, a cured thickness of 0.11 mm. The material properties of T300 fibre and LTM45 resin are given in Table 1. The material has no gap between the yarns, and has a low crimp angle of about 2 deg.
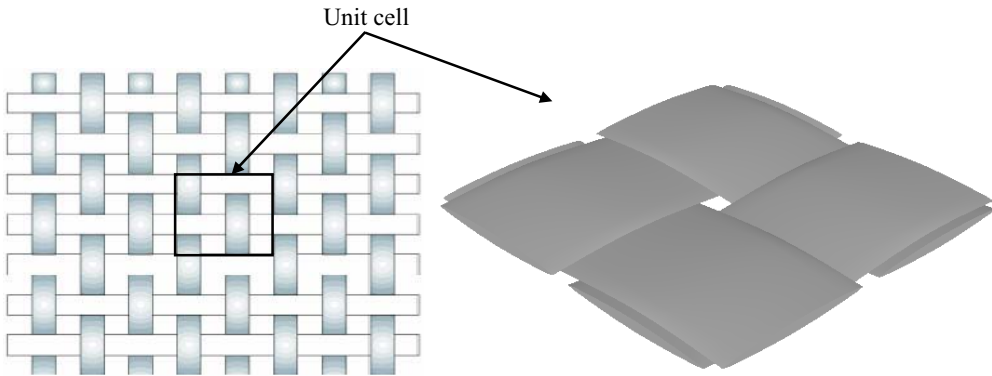
Unit cell

Figure 1. Plain weave composite and 3D solid model of unit cell

	T300	LTM45
E_1 [GPa]	230	3.1
E_2 [GPa]	14	3.1
G_{12} [GPa]	9	1.1
ν_{12}	0.2	0.41

Table 1. Material properties of T300 and LTM45.

The homogenized properties of the yarns can be obtained again by the contribution of the fibres and the matrix using the rule of mixtures as

$$E_1^y = V_f E_{1f} + E_m (1 - V_f) \tag{1}$$

where E_{1f} fibre longitudinal modulus, E_m resin elastic modulus, V_f fiber volume fraction. The rule of mixture yields the longitudinal modulus accurately but not the transverse modulus. For transverse modulus and shear modulus Halpin–Tsai equations are used as follows

$$E_2^y = E_3^y = \frac{\left(1 + \xi \eta V_f\right) E_m}{1 - \eta V_f} \tag{2}$$

where $\eta = \dfrac{E_{2f}/E_m - 1}{E_{2f}/E_m + \xi}$ and E_{2f} transverse modulus of fibres. ξ is a measure of fibre reinforcement, depending on the geometry of the fibres, packing and loading; $\xi = 2$ is taken as recommended for circular sections. The shear modulus of the yarn is obtained taking $\xi = 1$ in the Halpin–Tsai equations as follows

$$G_{12}^y = G_{13}^y = G_m \frac{\left(G_{12f} + G_m\right) + V_f\left(G_{12f} - G_m\right)}{\left(G_{12f} + G_m\right) - V_f\left(G_{12f} - G_m\right)} \tag{3}$$

where G_m and G_{12f} shear moduli of matrix and fibre, respectively. Major Poisson's ratio is calculated using volume fractions, and minor Poisson's ratio is obtained reciprocal relation as follows

$$\nu_{12}^y = \nu_{13}^y = V_y \nu_{12f} + \nu_m(1 - V_f) \tag{4}$$

$$\nu_{21}^y = \nu_{12}^y \frac{E_2^y}{E_1^y} \tag{5}$$

The material properties of the yarn are calculated using data in Table 1 and Eqs. 1 to 5 as follows: $E_1^y = 116.55$ GPa, $E_2^y = E_3^y = 6.54$ GPa, $G_{12}^y = G_{13}^y = 2.51$ GPa, $\nu_{12}^y = \nu_{13}^y = 0.305$, $\nu_{21}^y = 0.017$.

Finite element model and flexure failure

The warp and weft yarns are assumed to have a sinusoidal form with a period of L=2.75 mm and an amplitude of $t/4$ in Fig.2. The unit cell is modeled by initially curved beams, representing the two warp and two weft yarns in Fig.3. The beams have the properties of the orthotropic yarns, and equivalent rectangular cross section with $L/2 \times t/2$ (1.375×0.055 mm). The ends of the beams are denoted as P_i's, and to be used for boundary conditions. The interlaced yarns are constrained at the four crossover points, representing the bonding between the yarns, and transferring loads from one yarn to another. Kinematic constraints are imposed at the coupling nodes of the crossover points. Three rotational and three displacement degrees of freedom are constrained by eliminating the specified degrees of freedom at the coupling nodes in Abaqus. The mid-plane of the model is represented by dotted line.

The boundary conditions of the unit cell are assumed to be periodic, because the unit cell of the composite is only a basic repeating unit of the macro structure, which is obtained by repeating the unit cell longitudinal and transverse as well as through the thickness as many as needed. The effect of boundary conditions on the woven composite with finite dimensions is eliminated by the periodic boundary conditions. The unit cell is homogenized as a thin plate based on Kirchhoff's assumptions as used in CLT. The mid-plane strains ε_{ij} and curvatures κ_{ij} are related to change of displacement Δu_i^k and rotations $\Delta \theta_i^k$ of opposite boundaries as follows

$$\Delta u_i^k = \varepsilon_{ij} \Delta l_i \tag{6}$$

$$\Delta \theta_i^k = \kappa_{ij} \Delta l_i \tag{7}$$

where Δl_i is the distance between the two opposite nodes on the boundaries, representing the period along x or y direction.
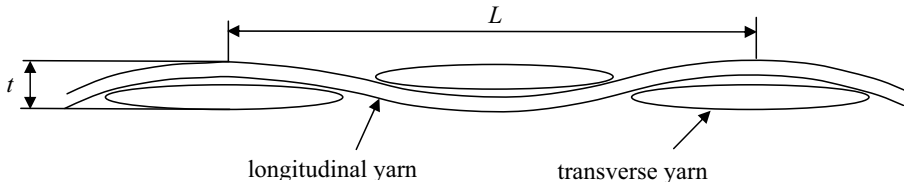
Figure 2. Schematic longitudinal cross section
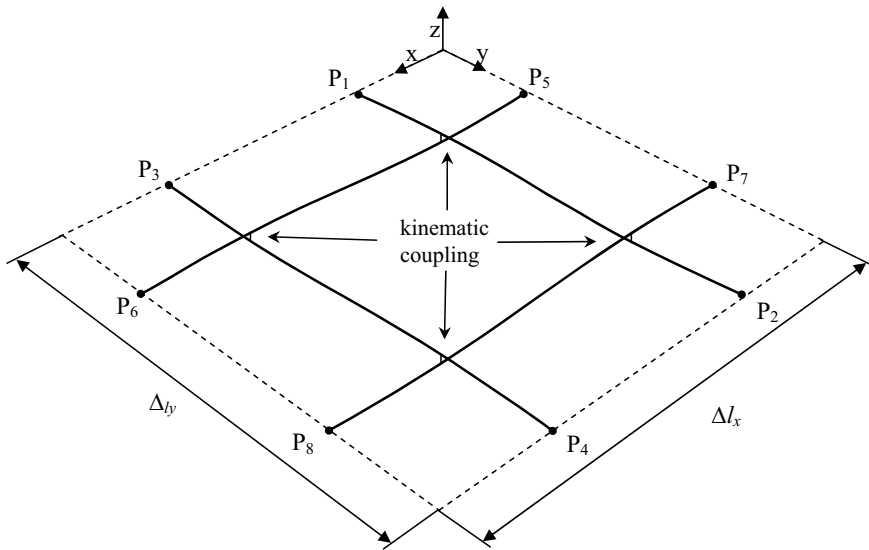
Figure 3. FE model of the unit cell

The constitutive equations of the homogenized plate relate mid-plane force N and moment M resultants to mid-plane strain and curvatures as follows

$$
\left\{ \begin{array}{c} N \\ \cdots \\ M \end{array} \right\} = \left[\begin{array}{ccc} A & \vdots & B \\ \cdots & & \cdots \\ B & \vdots & D \end{array} \right] \left\{ \begin{array}{c} \varepsilon \\ \cdots \\ \kappa \end{array} \right\} \tag{8}
$$

where A, B, D are matrices for extension, bending-extensional coupling, and bending stiffnesses. The periodic boundary conditions in Table 2 and 3 are applied to the nodes on the opposite side on the model. Four fixed dummy nodes that are not attached to any element of the model are defined as reference points RP1, RP2, RP3, and RP4 at the undeformed position of the boundary points P2, P4, P6, and P8, respectively. Then the boundary condition is taken as a constraint in Abaqus and the displacements or rotations are applied to the dummy nodes. In order to calculate A_{11}, the first deformation mode is assumed, i.e. $\varepsilon_{xx} = \delta_x / \Delta l_x$ and $\varepsilon_{yy} = \varepsilon_{xy} = \kappa_{xx} = \kappa_{yy} = \kappa_{xy} = 0$ hence the resultant forces and moments become $N_x = A_{11}\varepsilon_{xx}$ and $N_y = N_{xy} = M_x = M_y = M_{xy} = 0$. RP3 and RP4 are subject to prescribed displacement of δ_x along x-direction, corresponding constraint equations for the boundary nodes on the warp and weft direction can be written as

$$u_x^6 - u_x^5 - u_x^{RP3} = 0, \quad u_y^6 - u_y^5 = 0, \quad u_z^6 - u_z^5 = 0, \quad \theta_x^6 - \theta_x^5 = 0, \quad \theta_y^6 - \theta_y^5 = 0, \quad \theta_z^6 - \theta_z^5 = 0,$$
$$u_x^8 - u_x^7 - u_x^{RP4} = 0, \quad u_y^8 - u_y^7 = 0, \quad u_z^8 - u_z^7 = 0, \quad \theta_x^8 - \theta_x^7 = 0, \quad \theta_y^8 - \theta_y^7 = 0, \quad \theta_z^8 - \theta_z^7 = 0,$$
$$u_x^2 - u_x^1 = 0, \quad u_y^2 - u_y^1 = 0, \quad u_z^2 - u_z^1 = 0, \quad \theta_x^2 - \theta_x^1 = 0, \quad \theta_y^2 - \theta_y^1 = 0, \quad \theta_z^2 - \theta_z^1 = 0,$$
$$u_x^4 - u_x^3 = 0, \quad u_y^4 - u_y^3 = 0, \quad u_z^4 - u_z^3 = 0, \quad \theta_x^4 - \theta_x^3 = 0, \quad \theta_y^4 - \theta_y^3 = 0, \quad \theta_z^4 - \theta_z^3 = 0,$$

(9)

	$u_x^6 - u_x^5$ and $u_x^8 - u_x^7$	$u_y^6 - u_y^5$ and $u_y^8 - u_y^7$	$u_z^6 - u_z^5$ and $u_z^8 - u_z^7$	$\theta_x^6 - \theta_x^5$ and $\theta_x^8 - \theta_x^7$	$\theta_y^6 - \theta_y^5$ and $\theta_y^8 - \theta_y^7$	$\theta_z^6 - \theta_z^5$ and $\theta_z^8 - \theta_z^7$
$\varepsilon_{xx} = \delta_x / \Delta l_x$	δ_x	0	0	0	0	0
$\varepsilon_{yy} = \delta_y / \Delta l_y$	0	0	0	0	0	0
$\varepsilon_{xy} = 2\delta_x / \Delta l_x$	0	$\delta_x \Delta l_y / \Delta l_x$	0	0	0	0
$\kappa_{xx} = \delta_\theta \Delta l_x$	0	0	0	0	δ_θ	0
$\kappa_{yy} = \delta_\theta \Delta l_y$	0	0	0	0	0	0
$\kappa_{xy} = -2\delta_\theta / \Delta l_x$	0	0	$-\delta_\theta \Delta l_x / 4$ and $-3\delta_\theta \Delta l_x / 4$	δ_θ	0	0

Table 2. Boundary conditions along warp direction.

	$u_x^2 - u_x^1$ and $u_x^4 - u_x^3$	$u_y^2 - u_y^1$ and $u_y^4 - u_y^3$	$u_z^2 - u_z^1$ and $u_z^4 - u_z^3$	$\theta_x^2 - \theta_x^1$ and $\theta_x^4 - \theta_x^3$	$\theta_y^2 - \theta_y^1$ and $\theta_y^4 - \theta_y^3$	$\theta_z^2 - \theta_z^1$ and $\theta_z^4 - \theta_z^3$
$\varepsilon_{xx} = \delta_x / \Delta l_x$	0	0	0	0	0	0
$\varepsilon_{yy} = \delta_y / \Delta l_y$	0	δ_y	0	0	0	0
$\varepsilon_{xy} = 2\delta_x / \Delta l_x$	δ_x	0	0	0	0	0
$\kappa_{xx} = \delta_\theta / \Delta l_x$	0	0	0	0	0	0
$\kappa_{yy} = \delta_\theta / \Delta l_y$	0	0	0	δ_θ	0	0
$\kappa_{xy} = -2\delta_\theta / \Delta l_y$	0	0	$-\delta_\theta \Delta l_y / 4$ and $-3\delta_\theta \Delta l_y / 4$	0	$-\delta_\theta \Delta l_y / \Delta l_x$	0

Table 3. Boundary conditions along weft direction.

The model is meshed using two-node cubic beam elements B33 with an approximate element size of 0.01 mm. The total number of elements of the model is 1104. Static nonlinear analyses are carried out to find the stiffnesses. The stiffnesses are then obtained using the reaction forces and moments at the reference points and applying virtual work principal as in Table 4.

The strains at any point in the homogenized plate according to CLT are calculated as follows:

$$\begin{bmatrix} \varepsilon_x \\ \varepsilon_y \\ \varepsilon_{xy} \end{bmatrix} = \begin{bmatrix} \varepsilon_x^0 \\ \varepsilon_y^0 \\ \varepsilon_{xy}^0 \end{bmatrix} + z \begin{bmatrix} \kappa_x \\ \kappa_y \\ \kappa_{xy} \end{bmatrix}$$

(10)

where ε^0 and κ are mid-plane strains and the curvatures respectively. The maximum strain criterion assumes that material failure occurs when the in-plane strains along the principal material direction exceed the ultimate strains of the material as

$$
\begin{aligned}
-\varepsilon_L^{(-)} &< \varepsilon_1 < \varepsilon_L^{(+)} \\
-\varepsilon_T^{(-)} &< \varepsilon_2 < \varepsilon_T^{(+)} \\
|\gamma_{12}| &< \varepsilon_{LT}
\end{aligned}
\tag{11}
$$

where $\varepsilon_L^{(-)}$ and $\varepsilon_L^{(+)}$ are the longitudinal ultimate strains in compression and tension; $\varepsilon_T^{(-)}$ and $\varepsilon_T^{(+)}$ are the transverse ultimate strains in compression and tension; and ε_{LT} is the ultimate shear strain. When B_{ij} is zero and the plate is subject to only longitudinal curvature κ_x, corresponding bending moment and strain become $M_x = D_{11}\kappa_x$ and $\varepsilon_x = z\kappa_x$. When a unidirectional laminated plate is bent along its principal material direction, the maximum strain occurs on the outer edges of the plates, hence at $z = t/2$. Therefore, the maximum moment can be obtained from the ultimate strain ε_{max} (which is equal to the smaller in magnitude of ε_L^- or ε_L^+) as $M_x^{max} = 2\varepsilon_{max}D_{11}/t$.

Load case	Stiffness
$\varepsilon_{xx} = \delta_x / \Delta l_x$ and $\varepsilon_{yy} = \varepsilon_{xy} = \kappa_{xx} = \kappa_{yy} = \kappa_{xy} = 0$	$A_{11} = \dfrac{N_x}{\varepsilon_{xx}} = \dfrac{\left(F_x^{RP3} + F_x^{RP4}\right)/\Delta l_y}{\delta_x / \Delta l_x} = \dfrac{\Delta l_x}{\Delta l_y}\dfrac{\left(F_x^{RP3} + F_x^{RP4}\right)}{\delta_x}$
$\varepsilon_{yy} = \delta_y / \Delta l_y$ and $\varepsilon_{xx} = \varepsilon_{xy} = \kappa_{xx} = \kappa_{yy} = \kappa_{xy} = 0$	$A_{22} = \dfrac{N_y}{\varepsilon_{yy}} = \dfrac{\left(F_y^{RP1} + F_y^{RP2}\right)/\Delta l_x}{\delta_y / \Delta l_y} = \dfrac{\Delta l_y}{\Delta l_x}\dfrac{\left(F_y^{RP1} + F_y^{RP2}\right)}{\delta_y}$
$\varepsilon_{xx} = \delta_x / \Delta l_x$, $\varepsilon_{yy} = \delta_y / \Delta l_y$ and $\varepsilon_{xy} = \kappa_{xx} = \kappa_{yy} = \kappa_{xy} = 0$	$A_{12} = \dfrac{N_x - A_{11}\varepsilon_{xx}}{\varepsilon_{yy}} = \dfrac{\left(F_x^{RP3} + F_x^{RP4}\right)/\Delta l_y - A_{11}\delta_x/\Delta l_x}{\delta_y / \Delta l_y}$
$\varepsilon_{xy} = 2\delta_x / \Delta l_x$ and $\varepsilon_{xx} = \varepsilon_{yy} = \kappa_{xx} = \kappa_{yy} = \kappa_{xy} = 0$	$A_{66} = \dfrac{N_{xy}}{\varepsilon_{xy}} = \dfrac{\left(F_y^{RP3} + F_y^{RP4}\right)/\Delta l_y}{2\delta_x / \Delta l_x} = \dfrac{\Delta l_x}{\Delta l_y}\dfrac{\left(F_y^{RP3} + F_y^{RP4}\right)}{2\delta_x}$
$\kappa_{xx} = \delta_\theta / \Delta l_x$ and $\varepsilon_{xx} = \varepsilon_{yy} = \varepsilon_{xy} = \kappa_{yy} = \kappa_{xy} = 0$	$D_{11} = \dfrac{M_x}{\kappa_{xx}} = \dfrac{\left(M_x^{RP3} + M_x^{RP4}\right)/\Delta l_y}{\delta_\theta / \Delta l_x} = \dfrac{\Delta l_x}{\Delta l_y}\dfrac{\left(M_x^{RP3} + M_x^{RP4}\right)}{\delta_\theta}$
$\kappa_{yy} = \delta_\theta / \Delta l_y$ and $\varepsilon_{xx} = \varepsilon_{yy} = \varepsilon_{xy} = \kappa_{xx} = \kappa_{xy} = 0$	$D_{22} = \dfrac{M_y}{\kappa_{yy}} = \dfrac{\left(M_x^{RP1} + M_x^{RP2}\right)/\Delta l_x}{\delta_\theta / \Delta l_y} = \dfrac{\Delta l_y}{\Delta l_x}\dfrac{\left(M_y^{RP1} + M_y^{RP2}\right)}{\delta\theta}$
$\kappa_{xx} = \delta_\theta / \Delta l_x$, $\kappa_{yy} = \delta_\theta / \Delta l_y$ and $\varepsilon_{xx} = \varepsilon_{yy} = \varepsilon_{xy} = \kappa_{xy} = 0$	$D_{12} = \dfrac{M_x - D_{11}\kappa_{xx}}{\kappa_{yy}} = \dfrac{\left(M_x^{RP3} + M_x^{RP4}\right)/\Delta l_y - D_{11}\delta_\theta/\Delta l_x}{\delta_\theta / \Delta l_y}$
$\kappa_{xy} = -2\delta_\theta / \Delta l_x$ and $\varepsilon_{xx} = \varepsilon_{yy} = \varepsilon_{xy} = \kappa_{xx} = \kappa_{yy} = 0$	$D_{66} = \dfrac{M_{xy}}{\kappa_{xy}} = \dfrac{\left(M_x^{RP3} + M_x^{RP4}\right)/\Delta l_y}{-2\delta_\theta / \Delta l_x} = \dfrac{-\Delta l_x}{\Delta l_y}\dfrac{\left(M_x^{RP3} + M_x^{RP4}\right)}{2\delta_\theta}$

Table 4. Load cases and calculation of stiffnesses.

Results

Static nonlinear analyses are carried out to find the stiffnesses. The numerical results are given in Tables 5 and 6 along with published data. Since the bending-extensional coupling B_{ij} is zero, is not presented here. The effective stiffnesses of the plain weave composite were calculated analytically based on a mosaic model in [11]. As expected, in-plane properties are in agreement. The present stiffnesses are lower particularly for the stiffnesses A_{11} and D_{11}, but are expected to be more accurate because the crimp of the fibers and nonlinear effects were ignored in the mosaic model. Note that $A_{16}, A_{26}, D_{16}, D_{26}$ are zero in both the mosaic model and the present results and D_{12} is small in the results. Present results are also compared with those of the direct application of CLT [7], D_{11} of which is very high with a factor of 4. Therefore CLT should not be used to obtain bending stiffness directly. Adapted form of CLT as in the mosaic model is able to reduce the stiffness error significantly. The present result is in good agreement with that of Ref. [7], in which a similar FE model without periodic boundary conditions was used. Present model considers only the unit cell with periodic boundary conditions therefore the effect of modeling size does not appear, also it reduces modeling and computation time significantly.

Bending moment versus maximum strain is given in Fig.4. In parallel to the bending stiffness, the ultimate moments of the single-ply composite are quite different. When $\varepsilon_{\max}$ =0.015 is taken as the ultimate strain of the fiber, CLT yields a bending moment and curvature, which are higher and lower respectively with a factor of 4 compared with the FE results.

	$A_{11} = A_{22}$ (N/mm)	A_{12} (N/mm)	$A_{16} = A_{26}$ (N/mm)	A_{66} (N/mm)
present	5955.9	470.2	0.00	352.5
mosaic model [11]	6805.2	220.4	0.00	276.4

Table 5. Homogenized in-plane stiffnesses of single ply T300/LTM45.
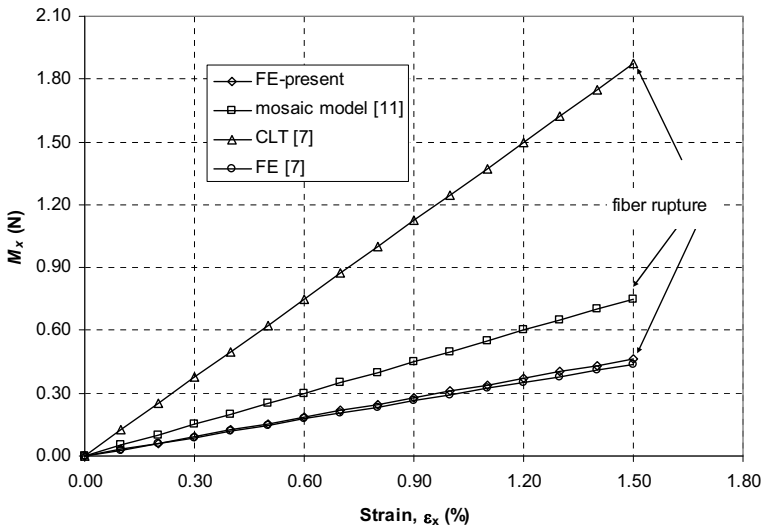
Figure 4. Bending moment vs strain.

	$D_{11} = D_{22}$ (Nmm)	D_{12} (Nmm)	$D_{16} = D_{26}$ (Nmm)	D_{66} (Nmm)
present	1.70	0.00	0.00	0.26
mosaic model [11]	2.75	0.09	0.00	0.28
FE [7]	1.61	-	-	-
CLT [7]	6.86	-	-	-

Table 6. Homogenized bending stiffnesses of single ply T300/LTM45.

Conclusions

A finite element model based on a unit cell of plain-weave T300/LTM45 composite is presented in this paper. The FE model uses initially curved beam elements to model the warp and weft yarns of the unit cell. Because the model uses only beam elements and periodic boundary conditions, it is simple yet captures the flexural stiffness accurately, also offers modeling ease and significant savings in computational time. Estimation of the flexural failure of the composite depends on the accurate estimation of the flexural stiffness of the composite. Direct application of CLT should not be used to predict the flexural failure as demonstrated. The present results are compared with those available in the literature. The model can also be extended for other weave styles as well as braided and stitched composites.

Acknowledgement

References

[1] R.A. Naik: Analysis of woven and braided fabric reinforced composites, NASA CR 194930, (1994).

[2] V. Carvelli, C. Poggi: A homogenization procedure for the numerical analysis of woven fabric composites, composites: Part A Vol. 32 (2001), pp.1425-1432.

[3 B.H. Le Page, F.J. Guild, S.L. Ogin, P.A. Smith: Finite element simulation of woven fabric composites, Composites: Part A Vol.35 (2004), pp. 861–872.

[4] G. Karami, M. Garnich: Effective moduli and failure considerations for composites with periodic fiber waviness, Composite Structures Vol. 67 (2005), pp.461–475.

[5] P. Xue, J. Cao, J. Chen: Integrated micro/macro-mechanical model of woven fabric composites under large deformation, Composite Structures Vol. 70 (2005), pp. 69–80.

[6] R. Akkerman: Laminate mechanics for balanced woven fabrics, Composites: Part B Vol. 37 (2006), pp.108–116.

[7] O. Soykasap: Micromechanical models for bending behavior of woven composites, Journal of Spacecraft and Rockets Vol. 43 (2006), pp. 1093-1100.

[8] R.L. Karkkainen, B.V. Sankar: A direct micromechanics method for analysis of failure initiation of plain weave textile composites, Composites Science and Technology Vol. 66 (2006), pp. 137–150.

[9] ABAQUS/Standard User's Manual, Version 6.7, Pawtucket, RI, USA, (2007).

[10] A.B.H. Kueh, S. Pellegrino: ABD Matrix of Single-Ply Triaxial Weave Fabric Composites, Proceeding of 48th AIAA/ASME/ASCE/AHS/ASC Structures, Structural Dynamics and Materials Conference, Honolulu, Hawaii (2007).

[11] O. Soykasap: Analysis of plain weave composites, Proceeding of XV international conference on mechanics of composite materials, Riga, Latvia (2008).